Disease development is accompanied by changes in bacterial protein abundance and functions in a refined model of dextran sulfate sodium (DSS)-induced colitis

Sven-Bastiaan Haange[1,3#], Nico Jehmlich[1#], Maximilian Hoffmann[2#], Klaus Weber[4], Jörg Lehmann[2], Martin von Bergen[1,3*], Ulla Slanina[2]

[1]Helmholtz-Centre for Environmental Research - UFZ, Department of Molecular Systems Biology, Leipzig, Germany

[2]Fraunhofer Institute for Cell Therapy and Immunology, Department of Therapy Validation, Leipzig, Germany

[3]University of Leipzig, Faculty of Life Sciences, Institute of Biochemistry, Leipzig, Germany

[4]AnaPath GmbH, Liestal, Switzerland

# These authors contributed equally to this work

ORCID - ID

Sven-Bastiaan Haange: 0000-0003-2952-1152

Nico Jehmlich: 0000-0002-5638-6868

Maximilian Hoffmann: 0000-0002-5186-7232

Klaus Weber

Jörg Lehmann

Martin von Bergen: 0000-0003-2732-2977

Ulla Slanina (née Schwertassek): 0000-0003-4215-3833

*Correspondence:

Prof. Dr. Martin von Bergen
Tel: +49-341-235-1211

ABSTRACT

Using the acute dextran sulfate sodium (DSS)-induced colitis model, studies have demonstrated that intestinal inflammation is accompanied by major changes in the composition of the intestinal microbiota. Only little is known about the microbial changes and more importantly their functional impact in the chronic DSS colitis model. We used a refined model of chronic DSS-induced colitis that reflects typical symptoms of the human disease without detrimental weight loss usually observed in DSS models. We sampled cecum and colon content as well as colon mucus from healthy and diseased mouse cohorts (n=12) and applied 16S rRNA gene sequencing and metaproteomics. An increase of *Prevotella* sp. in both colon content and mucus were observed. Functional differences were observed between sample types demonstrating the importance of separately sampling lumen content and mucus. The abundance of *Desulfovibrio*, a sulfate-reducing bacterium, was positively associated with the carbon metabolism. *Lachnoclostridium* was positively correlated to both vitamin B6 and tryptophan metabolism. In summary, functional changes in the distal colon caused by DSS treatment were more pronounced in the mucus-associated microbiota than in the microbiota present in the distal colon content.

Keywords: Dextran sulfate sodium (DSS); colitis; mouse model; metaproteomics; microbiota

INTRODUCTION

The intestinal microbiota plays a pivotal role in protecting the host against pathogenic microbes as well as having an impact on the immune system and the metabolism of the host[1]. In this respect, the most important question does not concern the identity of the microbes, but more importantly the functional effects of their metabolism. Microbes have a vast repertoire of metabolic functions and they can greatly alter their metabolism in response to changing environmental factors[2]. These functional changes can considerably impact the host's metabolism and immune system and hence have implications in various diseases[3].

Inflammatory bowel diseases (IBD), with the major clinical forms of Crohn's disease (CD) and ulcerative colitis (UC), are chronic-remitting inflammatory disorders of the intestinal tract. Symptoms include abdominal cramps, bloody diarrhea and weight loss, and extra-intestinal manifestations are possible[4]. The etiology of IBD is so far unknown, but most likely includes an aberrant response of the host's immune system to the gut microbiota[5, 6]. The microbial composition of the intestine can be significantly changed in IBD patients[7, 8]. However, it has not been elucidated whether this change is cause or consequence of the chronic intestinal inflammation. The changes in microbial composition are also reflected by functional alterations: Comparative metaproteomics in stool samples from six twin pairs with or without CD revealed significant changes in protein abundance for more than 100 functional groups, including the depletion of proteins involved in short-chain fatty acid (SCFA) production in CD patients[9].

The mouse model of dextran sulfate sodium (DSS)-induced colitis is the most widely used inducible animal model in IBD research, both for studying pathogenesis and for testing the efficacy of new therapeutics[10]. DSS is a water-soluble polysaccharide that in combination with short-chain fatty acids derived as a product of bacteria metabolism damages the epithelial monolayer of the colon. This presumably results in reduced barrier function of the epithelium and allows infiltration of pro-inflammatory intestinal antigens (e.g. whole bacteria or bacterial components) into the underlying tissue[11]. In the DSS colitis model, the epithelial damage and resulting inflammation is restricted to the colon, with a potential influence on the microbial composition in the adjacent cecum. Several studies have reported changes of the gut microbiota in the DSS colitis model and other mouse models of IBD[12]. Furthermore, metaproteomics analysis of the gut microbiota in a mouse model of CD demonstrated that disease severity and location are microbiota-dependent, with clear evidence for the causal role of bacterial dysbiosis in the development of chronic ileal inflammation[13].

Several strategies for microbial community analysis have been developed that complement and expand traditional genomic profiling[14]. These include the analysis of data types that better reflect the functional activity of the microbiota, such as metatranscriptomics,

metaproteomics or metabolomics. This has led to improved mechanistic models of structure and function of the microbial community[15]. Metaproteome analyses have provided unprecedented in-depth characterization of the taxonomic composition and functionality of microbial communities. Applying these techniques, we will obtain further insight into the gut microbiota and its response to DSS treatment. Currently, metaproteomics is potentially the analysis that most accurately determines the function with respect to translation, energy and carbohydrate metabolism, as well as antimicrobial defense[16, 17]. Identified proteins can be assigned to taxa as well as functional properties. Thus, metaproteomics is an optimal method to investigate the functional repertoire of the gut microbiota[18].

We have developed a refined model of chronic DSS-induced colitis that reflects typical symptoms of human IBD without a risky body weight loss usually observed in DSS models[19]. In this study, we used metaproteomics to characterize the disease-related changes in bacterial protein abundance and functions in the refined model of DSS colitis. To assess structural and functional changes, we applied 16S rRNA gene sequencing and metaproteomics analysis of the intestinal microbiota in three different entities of the intestinal environment, i.e. colon mucus, colon content and cecum content.

METHODS

Animals

Female BALB/cJRj mice (11 weeks old; 20-24 g) were purchased from Janvier (Saint-Berthevin, France). Mice were housed as six animals per cage in a temperature- and light/dark cycle-controlled environment (23°C, 12 h/12 h light/dark, 50 % humidity). They had free access to pelleted standard rodent chow and water *ad libitum*. Animals were acclimatized to the environmental conditions for 14 days before starting of treatment. To each group, 12 animals were assigned randomly. All experimental procedures were approved by the State Animal Care and Use Committee (Landesdirektion Sachsen, Leipzig, Germany, TVV 24/14) and were carried out in accordance with the European Communities Council Directive (86/609/EEC) for the Care and Use of Laboratory Animals. All efforts were made to minimize suffering of the animals.

Induction of chronic DSS colitis

Chronic DSS colitis was induced as described [19]. Briefly, a dose of 2 % DSS (MW 36,000-50,000 Da; Lot No. M7191; MP Biomedicals, Santa Ana, USA) was administered in autoclaved drinking water (w/v) for 7 days, followed by administration of 1 % DSS for 10 days and 2 % DSS for another 7 days. DSS solutions were changed every 3 to 4 days. Animals were monitored daily for overall physical and behavioral appearance, and body weight loss as well as scores for stool consistency and blood in stool were assessed. The clinical score was calculated as the average of the scores for body weight loss, stool consistency, and blood in stool.

Dissection

On day 25, animals (n=12 per group) were sacrificed in deep anaesthesia using carbon dioxide. The colon was dissected and its length from cecum to anus was determined. The content of the cecum was removed and frozen on dry ice. Two parts of 0.3 to 0.5 cm of the most distal colon were transferred into 4 % phosphate-buffered formaldehyde and fixed for 24 h prior to preparation for histological analysis. The remaining part of the colon was cut longitudinally and content from the distal part was removed and frozen on dry ice. Mucus from the distal colon was collected by scraping with a spatula, placing in 100 µL of Tris buffer (50 mM Tris, 5 mM EDTA, 50 mM NaCl, pH 8) and freezing on dry ice.

Histological analysis

Fixed tissue samples were dehydrated in grade ethanol followed by isopropanol and xylol, and embedded in paraffin. Tissue sections were cut at an approximate thickness of 3 µm using a rotary microtome (LEICA RM2255, Nussloch, Germany), mounted on glass slides and dried on a hotplate (70°C). Sections were dewaxed, hydrated, and stained with

haematoxylin and eosin (H&E). Images were taken from selected samples and digitized using an image scanner (Zeiss AxioScan.Z1; Zeiss, Jena, Germany). Stained sections were evaluated by a trained pathologist with regard to the extent of inflammation, edema, and superficial necrosis, as well as the infiltration of granulocytes, lymphocytes, and macrophages into the tissue.

For immunofluorescent analysis, dewaxed and rehydrated tissue sections were subjected to heat- or proteolysis-induced antigen retrieval using Tris-EDTA-buffer (pH 9) at 97 °C for 25 min or proteinase K at 37°C for 5 min. Sections were washed and blocked with 1 % fetal bovine serum (FBS) in phosphate-buffered saline (0.05 % Tween20, Sigma-Aldrich, Taufkirchen, Germany; PBS-T) for 30 min. Blocked samples were incubated with primary antibodies (polyclonal cross-reactive rabbit anti-human CD3, Dako, Hamburg, Germany; monoclonal rat anti-mouse F4/80, purified from hybridoma supernatants; polyclonal rabbit anti-mouse MPO, Abcam, Cambridge, UK) at a dilution of 1:50 to 1:1000 at room temperature (RT) for 2 h or at 4°C overnight, respectively. After washing with PBS-T, slides were incubated with the corresponding secondary antibody (goat anti-rabbit IgG, carbocyanine (Cy)3-conjugated, Dianova, Hamburg, Germany) at a dilution of 1:200 to 1:500 at room temperature for 1 h. Stained sections were washed and mounted with a 4′,6 diamidin-2-phenylindol (DAPI)-containing mounting medium (Fluoroshield™ with DAPI; Sigma-Aldrich). Images were taken and digitized using an image scanner (Zeiss AxioScan.Z1; Zeiss) and quantification was done with ImageJ software (v1.46r; Wayne Rasband, National Institutes of Health). Signals for Cy3 and DAPI were measured in a defined region of interest (ROI) applying constant greyscale limits. Expression of the markers was presented as Cy3-positive area relative to the DAPI-positive area [%]. For each treatment group, two sections per animal were analyzed.

Preparation of bacterial lysates

Samples from cecum content, distal colon content and distal colon mucus were thawed and resuspended in 1 mL lysis buffer (50 mM Tris, 5 mM EDTA, 0.4 % SDS, 50 mM NaCl, 1 mM PMSF, pH 8). Lysis was done using bead beating (FastPrep-24, MP Biomedicals, Santa Ana, CA, USA; parameters were set to 5.5 ms, 3x with a duration of 1 min, 4°C), followed by heating to 60 °C for 15 min (Thermomixer comfort 5355, Eppendorf, Eppendorf, Hamburg, Germany; at 60 °C with shaking at 1,400 rpm) and disintegration with a sonic probe (UP50H, Hielscher, Teltow, Germany; 2x cycle 0.5 and amplitude 60 %). Samples were spun at 10,000 rpm, 10 min, 4°C. Supernatants (= bacterial lysates) containing bacterial DNA and protein were kept and stored at -20°C.

DNA extraction and 16S rRNA gene sequencing

500 µL of bacterial lysate from cecum (n=8), distal colon content (n=8), or distal colon mucus (DSS: n=7; control n=8) were used for DNA purification. 260 µL NH_4 acetate (10 M) were added, samples were incubated on ice for 5 min and spun at 13,000 rpm, 10 min, 4°C. An equal volume of ultra-pure isopropanol was added to the supernatant, mixed thoroughly and incubated on ice for 30 min. Samples were centrifuged at 13,000 rpm, 10 min, 4°C, pellets were washed with 70 % Ethanol, vacuum-dried (SpeedVac) and resolved overnight in TE-Buffer (1 mM EDTA, 10 mM Tris, pH 8). DNA was purified and proteins removed using the QIAmp DNA Mini Kit (Qiagen, Valencia, CA USA) according to the manufacturer's instructions. DNA content was quantified using Nanodrop (NanoDrop2000, Thermo Fisher Scientific, Rockford, IL, USA).

16S rRNA gene library preparation and Illumina MiSeq amplicon sequencing was performed by Molecular Research DNA (MR DNA, Shallowater, TX, USA). The 16S rRNA gene V4 region was amplified with the barcoded primer pair 525/806 using the HotStarTaq Plus Master Mix Kit (Qiagen) using the following conditions: 94°C for 3 min; 28 cycles of 94°C for 30 sec, 53°C for 40 sec and 72°C for 1 min; 72°C for 5 min (total of 30 PCR cycles). After pooling of amplicons, sequencing was done on an Illumina MiSeq DNA sequencer (Illumina, San Diego, CA, USA) according to the manufacturer's instructions.

Protein preparation and LC-MS/MS analysis

Bacterial lysate (n=12, except for DSS distal colon content which was n=10) was used for protein purification and tryptic digest according to a modified procedure previously described[20]. Briefly, protein concentration was determined using a BCA protein assay kit (Pierce Protein Biology Products, Thermo Fisher Scientific). 40 µg (cecum and colon content samples) or 100 µg (colon mucus samples) of protein were precipitated in a 5-fold volume of acetone at -20°C overnight. Proteins were separated by SDS-PAGE: cecum and colon content samples were run approx. 5 mm into the separating gel and the whole gel lane was cut out into one fraction; the colon mucus samples were run 15 mm into the separating gel and each lane was cut into 3 separate fractions for greater coverage of proteins. Samples were further processed by in-gel reduction and alkylation of cysteine residues, in-gel tryptic digest and elution as well as desalting of tryptic peptides as previously described[20].

Samples were reconstituted in 0.1 % formic acid and peptide concentrations were determined using Nanodrop (NanoDrop2000, Thermo Fisher Scientific). For each LC-MS run, 1 µg of peptides was injected into a Nano-HPLC (UltiMate 3000, Dionex, Thermo Fisher Scientific). Peptides were first trapped for 3 min on a C18-reverse phase trapping column (Acclaim PepMap® 100, 75 µm x 2 cm, particle size 3 µM, nanoViper, Thermo Fisher Scientific), followed by separation on a C18-reverse phase analytical column (Acclaim

PepMap® 100, 75 µm x 25 cm, particle size 3 µM, nanoViper, Thermo Fisher Scientific) using a two-step gradient (90 min from 4 % to 30 % B, then 30 min from 30 % to 55 % B ; A: 0.1 % formic acid in MS-grade water; B: 80 % acetonitrile, 0.1 % formic acid in MS-grade water) with a solvent flow-rate of 300 nL/min and a column temperature of 35°C. Eluting peptides were ionized by a nano ion source (Advion Triversa Nanomate, Ithaca, NY, USA) and measured using a Q Exactive HF mass spectrometer (Thermo Fisher Scientific) with the following settings: MS resolution 120,000, MS automatic gain control (AGC) target 3,000,000 ions, maximum injection time for MS 80 ms, intensity threshold for MS/MS of 17,000 ions, dynamic exclusion 30 sec, TopN =20, isolation window 1.6 *m/z*, MS/MS resolution 15,000, MS/MS AGC target 50,000 ions, maximum injection time for MS/MS 120 ms.

Data analysis and statistics

All clinical data were analysed using Prism v6 for Windows (GraphPad Software, La Jolla, CA, USA). Line charts for clinical parameters are presented as mean ± SEM. Significant differences between these data sets were estimated by two-way analysis of variance (ANOVA). Scatter plots for colon length and histological analysis are presented as individual data points. Significant differences between these data sets were estimated by Kruskal-Wallis one-way ANOVA (if normally distributed) or by One-way ANOVA on Ranks (if the normality test failed). In case of normal distribution of data, the data sets were compared by the Holm-Sidak´s post-hoc test. If the normality test failed, the Dunnetts post-hoc test was applied. Values were considered significantly different if $P<0.05$, with $P<0.01$, $P<0.001$, or $P<0.0001$ denoting higher significance.

16S rRNA gene raw sequencing data was processed using QIIME[21] to assess quality of sequences, removal of barcodes and removal of sequences shorter than 150 bp. Sequences with ambiguous base calls were removed, sequences were denoised, operational taxonomic units (OTUs) generated and chimeras removed. OTUs were generated by clustering sequence reads to bins with 97 % sequence similarity. OTUs were classified to taxa by blasting them against a curated database derived from GreenGenes, RDPII [22] and NCBI (www.ncbi.nlm.nih.gov/). OTUs were classified to species if blast matches had similarities of greater than 97 %. Similarities of between 97 % and 95 % were annotated to unclassified genus, of between 95 % and 90 % annotated to unclassified family, of between 90 % and 85% annotated to unclassified order, of between 85 % and 80 % annotated to unclassified class, of between 80 % and 77 % annotated to unclassified phylum and of <77 annotated to unknown. Finally, relative numbers of reads were calculated for each taxon and the significance of differences in abundance for each taxon between DSS-exposed and control

mice was calculated by the independent two-sided Student`s *t* test. P values were corrected for multi-testing using the Benjamini-Hochberg method[23].

LC-MS spectra were searched using the Proteome Discoverer (v1.4; Thermo Fisher Scientific). Search settings were: Sequest HT search engine, trypsin (full specific), MS tolerance 10 ppm, MS/MS tolerance 0.02 Da, two missed cleavage sites, dynamic modifications oxidation (Met), static modifications carbamidomethylation (Cys). Only peptides that passed the FDR thresholds set in the Percolator node of <1 % FDR q value, and were rank 1 peptides, were considered for protein identification. Protein grouping was enabled, with protein group requiring at least one unique peptide. All protein-coding sequences of the identified bacteria genera from the 16S rRNA gene sequencing data and mouse were downloaded from UniProt (http://www.uniprot.org/) and were combined into a custom-made database. Label-free quantification was done using the Top-3 peptide area for approach. These linear area values were $\log_{10}$-transformed and median normalized. The fold changes were calculated and statistical significance was determined and corrected for multi-testing by the Benjamini-Hochberg using R[24]. Pathway analysis for bacterial protein groups was done using KEGG pathways[25]. Significance was calculated using the independent two-sided Student's *t* test.

Principal component analysis and non-metric multi-dimensional scaling (NMDS) plots and figures were calculated and constructed using R. Correlation analysis of data was done using the *corrplot R* package. Only significant correlation scores were investigated (P<0.01, Fisher's Z-transformation of Pearson's product moment correlation coefficient).

A *multi-level pattern analysis* was used to identify high-fidelity genera (from metaproteomics) that were significantly associated with DSS or control samples (in all three sections, i.e. cecum, distal colon content and distal colon mucus)[26]. The function *multipatt* was implemented in the R library *indicspecies*. The statistical significance of species site-group associations was calculated through random reassignment of groups (n=999 permutations) using *signassoc*.

RESULTS

DSS treatment induced chronicity of clinical symptoms reminiscent of IBD

To induce typical symptoms of chronic colitis, mice were given DSS in drinking water according to a regimen of alternating DSS concentrations over 25 days. A clinical score based on body weight loss, stool consistency and colonic haemorrhage was assessed daily. Compared to control animals receiving pure water, DSS-fed mice showed a significantly elevated clinical score starting from day 6. The clinical score reached a maximum at day 10

and stayed on a chronically elevated level until the end of the experiment (**Figure 1A**). DSS-fed mice lost up to 10 % of the initial body weight at the peak of clinical symptoms, but regained weight in the chronic phase of disease (**Figure 1B**). Thus, in the chronic phase, the clinical score was mostly determined by diarrhea and colonic hemorrhage. Whereas the stool almost initially became softer, diarrhea and colonic hemorrhage became apparent at days 5-7 and remained on a chronic level (**Figure 1C** and **D**). DSS-induced disintegration of the epithelium and the ensuing inflammatory response resulted in fibrosis and scarring of the colon tissue that was reflected by shortening of the colon. As expected from the clinical outcome, the colon length was significantly reduced in DSS-treated mice if compared to healthy control animals (**Figure 1E**).

Based on hematoxylin-eosin-stained cross sections of the distal colon, a histopathological score was evaluated, considering infiltrating lymphocytes, granulocytes and macrophages as well as the degree of edema and superficial necrosis. Tissue distribution of infiltrating immune cells was characterized in more detail by immunofluorescence staining for granulocytes (myeloperoxidase, MPO), macrophages (F4/80) and T cells (CD3) (**Figure 2A**). Consistent with the clinical parameters, the histopathological score was significantly elevated in DSS-treated mice (**Figure 2B**). As described for DSS models, the severity of tissue degeneration and inflammation increased from the proximal to the distal part of the colon. To characterize the nature and distribution of infiltrating immune cells in more detail, tissue cross sections were stained for typical cell markers and quantified as area positive for the respective antigen relative to the area of (4′,6 Diamidin-2-phenylindol) DAPI-positive nuclei (**Figures 2C-E**). Expression of MPO, a microbicidal enzyme produced by granulocytes, was significantly increased in DSS-treated mice if compared to the healthy control group (**Figure 2C**). Likewise, infiltration of F4/80^{+} macrophages (**Figure 2D**) and CD3^{+} T cells (**Figure 2E**) was significantly induced in DSS-treated animals. These results indicate that DSS treatment induced an immune response that was mainly driven by innate immune cells and T cells.

Diversity and structural composition of the microbiota differed between DSS-treated and healthy animals

Most of the information that is available on the diversity and structural composition of the intestinal microbiota is obtained from faecal samples that potentially reflect the community present in the lumen of the distal colon. We have chosen a different approach that aimed at the comparative analysis of the content of cecum and distal colon vs. the mucus derived from distal colon using 16S rRNA gene sequencing. In total, 5619 operational taxonomic units (OTUs) were identified (Supporting Information Table S3). An α-diversity analysis on taxonomic community structure revealed a significant decrease in richness in cecum and distal colon mucus in DSS-treated samples **(Figure 3A**). Evenness was only significantly

different in samples of the distal colon mucus, with an increase in DSS-treated samples (**Figure 3A**). Shifts in community structure between the microbiota of DSS-treated animals and healthy controls in mucus from distal colon, content from distal colon and cecum could be segregated in the Principal Component Analysis (PCA) plot of the Operational Taxonomic Units (OTUs) (**Figure 3B**). Distinct separation of the microbiota from DSS-treated and control animals was highly significant (P<0.001) as shown by non-metric multidimensional scaling (NMDS) plots. The stress values for the three NMDS plots were below 0.1, indicating a very good fit (**Figure 3C**).

In addition to qualitative changes, the relative abundance of 16S rRNA gene sequences was analyzed (**Figure 3D**). Out of eight bacterial phyla detected, Firmicutes were the most abundant in cecum content, occupying more than 90 % of reads in both control and DSS-treated animals. Likewise, Firmicutes was the most abundant phylum in distal colon content and mucus, followed by Bacteroidetes. The abundance of Firmicutes was significantly decreased in the distal colon mucus of DSS-treated animals, while Bacteroidetes increased in abundance. Changes in abundance were most prominent in the colon mucus, whereas in the content of the distal colon, no significant differences on the phyla level could be observed between DSS-treated and control animals. Moreover, only two phyla, Firmicutes and Actinobacteria, showed significantly higher and lower abundance, respectively, in the content samples of the cecum of DSS-treated versus healthy animals (**Figure 4**).

We further assessed the relative abundance with respect to the structural composition in the three different locations of the intestinal tract, with the heat-map demonstrating substantial differences (**Figure 4**). Several genera showed significant differences (P<0.05) in the abundance in the cecum content. The most notable genus was *Clostridium*, which was higher abundant in the cecum content, whereas e.g. *Lactobacillus* revealed a significantly lower abundance after DSS treatment. These findings suggest a remarkable reorganization of the microbial community in the cecum after DSS treatment. In the distal colon content, six genera were observed with significant differences between DSS-treated and control animals. For example, abundance of *Ruminococcus* was significantly lower after DSS treatment, whereas *Prevotella* was highly abundant in these animals. In the mucus-associated microbiota of the distal colon, nine genera showed significantly different levels between DSS-treated and control animals. For example, *Prevotella* showed a remarkably higher abundance with high significance (P<0.001, fold change >2) after DSS treatment. For *Lachnoclostridium,* a lower abundance was observed in the cecum content (P=0.011, fold-change<-2) and the distal colon mucus (P=0.0356, fold-change =-1.94) after DSS treatment (**Figure 4**).

Metaproteomics analysis revealed functional changes of the microbiota after DSS treatment

Having identified the changes in microbiota composition between DSS-treated and healthy animals, we applied a label-free shotgun metaproteomics approach to identify the protein core of the intestinal microbiota in the colon and cecum samples, as well as to assess potential functional differences of the microbiota in diseased vs. healthy animals.

In total, 5603 protein groups were identified in the cecum content, 6390 protein groups in the distal colon content and 7102 protein groups in the distal colon mucus. Depending on sample location, up to 50% of bacterial protein groups could not be assigned to a single phylum (Supporting Information Figure S1B). We analysed the α-diversity of samples based on Cluster of Orthologous Groups (COG) functions and found little change between DSS-treated and control samples in either richness or evenness (Supporting Information Figure S1B). The PCA-based clustering approach on the functional classes of COGs revealed a strong segregation by sample location (i.e. cecum content, colon content and colon mucus) and only a minor effect of treatment (DSS vs. control) (**Figure 5A**), indicating a strong location dependence of protein functionality. A pairwise view provided by the NMDS plots of the three sample types showed that DSS treatment significantly affected the abundance of protein functions (**Figure 5B**). Taken together, these results demonstrated that in addition to relevant alterations on the taxonomic level, changes on the functional levels could be observed in the intestinal microbiota of DSS-treated animals.

A multi-level pattern analysis was applied to determine key taxonomic indicators for DSS or control mice samples and to better understand the structural community composition after DSS treatment. This analysis included valuable information about the specificity and sensitivity of the indicator belonging to the site group (**Supporting Information Table S4**). Pairwise protein indicator analysis revealed that *Brevibacillus* (P=0.018, colon content and P=0.002, cecum content) was an indicator species for control samples, although only few proteins were identified. In contrast, *Corynebacterium* (P=0.008, cecum content) or *Alloprevotella* (p= 0.006, colon content) could be determined as taxonomic indicators for samples from DSS-treated animals. Notably, *Afipia* (P=0.019), an α-Proteobacterium that is suspected to cause infections was one of the indicators in colon mucus samples from DSS-treated animals[27]. The most affected KEGG metabolic pathways, which represent the basic functional level of the three sample sites, were depicted (**Figure 5C**). The selected minimum pathway coverage was 10 % and ranged from 10 % to 50 %. However, some pathways were comprised of few proteins, so that the coverage was only of limited benefit. After DSS treatment, we identified more protein groups of the lipid metabolism, biotin metabolism, and the degradation of aromatic compounds in cecum and colon content, if compared to colon

mucus. In contrast, protein groups assigned to the C5-branched dibasic acid metabolism showed a lower abundance in cecum and colon content after DSS treatment. We observed that the directions of the functional pathways were more similar between cecum and colon content and less similar if compared to colon mucus. The carbon metabolism in the colon mucus was strongly affected by DSS treatment. In addition, the amino acid metabolism (i.e. tryptophan) and the fatty acid metabolism displayed clear changes, suggesting a physiological effect in the metabolism of the colon-mucus associated microbiota.

Altered metabolic pathways significantly correlate and anti-correlate to specific bacterial genera

In order to measure the strength and direction of association between clinical and histopathological scores and the metaproteome data, we calculated the Pearson's product moment correlation. For the analysis, we only considered a statistically significant Pearson's product moment correlation coefficient with $P<0.01$ (**Figure 6**). Using this analysis, we observed several trends and directions: a negative correlation of the genera *Parvibacter* or *Enterorhabdus* (both Actinobacteria) were observed in all three localizations. The same could be observed for other genera (*Pedobacter* or *Nubsella*) from the phylum Bacteroidetes. In contrast, *Prevotella* showed a strong positive association with both clinical and histopathological score, especially in the mucus layer. At the functional level, a significant negative association in the general metabolic pathway of carbon metabolism was observed in the colon mucus, which indicated a functional dysbiosis in DSS-induced colitis. We also calculated the Pearson correlation analysis between the relative bacterial abundance (assessed by 16S rRNA gene sequencing) and the metabolic functions of the intestinal microbiota (assessed by metaproteomics) (**Figure 7**). The highest and strongest correlation was observed for the distal colon mucus. Interestingly, the carbon metabolism was positively associated with Proteobacteria at the phylum level. At the genus level, a positive association of the carbon metabolism was observed for *Desulfovibrio* (Proteobacteria), whereas *Bacteroides*, *Prevotella* (Bacteroidetes) and other Firmicutes (*Erysipelatoclostridium* or *Ruminiclostridium*) were negatively associated with the carbon metabolism. Remarkably, negative associations at the genus level were more prominent in cecum content, whereas more positive associations of the bacterial abundance to the metabolic pathway (e.g. aromatic compound degradation) were found in colon content. The correlation heat-map comprehensively showed the high bacterial metabolic versatility and the great dynamic of bacterial turnover in the intestinal tract, which was observed in the biotin metabolism. In cecum content, this metabolism showed predominantly negative statistical association to the majority of bacterial genera, whereas the opposite was observed for colon content. Moreover, several bacterial genera (e.g. *Lachnoclostridium* or *Prevotella*) showed different associations depending on the intestinal location. Furthermore, we observed positive

correlations of *Lachnoclostridium* with the tryptophan metabolism pathway and the vitamin B6 (cofactor in amino transferases) metabolic pathway in the colon mucus.

DISCUSSION

Numerous animal models are available for studying the pathological mechanisms of IBD or to evaluate the potential of new therapies. In IBD research, the acute DSS-induced colitis model is the most commonly applied mouse model. However, this model has several caveats such as the lack of a chronic adaptive immune response as well as severe body weight loss of the animals. Recently, we presented a refined mouse model of chronic DSS-induced colitis that reflects clinical symptoms of IBD without risky weight loss[19]. This model has already been successfully applied to evaluate the therapeutic effect of a sage and bitter apple extract in DSS colitis[28].

To further characterize the refined DSS model, the gut microbiota was analyzed on a taxonomic and functional level in the colon of healthy and diseased mice using 16S rRNA gene amplicon sequencing and metaproteomics. Previous studies have already analyzed gut microbiota composition in different variants of the DSS model using bacterial 16S rRNA gene amplicon sequencing and/or metatranscriptomics[29, 30]. These studies revealed that even short colitis episodes were detectable in the microbiota composition. Already after one episode of acute colitis, a signature of microbiota dysbiosis was detectable[29], which became more pronounced after repeated cycles of DSS treatment[30]. However, both studies reported a remarkable resistance and resilience of the intestinal microbiota to inflammation-induced dysbiosis. Consistent with previous studies, the intestinal microbiota in the refined DSS model was dominated by Firmicutes and Bacteroidetes. However, in contrast to another study, the phylum Verrucomicrobia was not detected, probably due to variations associated with the host phenotype[31]. We observed several significant changes on the taxonomic level in cecal and colon content samples which was in agreement with recent studies [32]. In the colon mucus, the abundance of Actinobacteria was significantly reduced after the onset of DSS-induced colitis, which was not been observed in previous studies. Controversial results have been obtained from experiments using the same mouse strain under similar conditions. The initial intestinal gut microbiota had a profound influence on the DSS-induced colitis. Changes in the microbial community composition after DSS treatment were shown to occur with parallel changes in diversity[33]. *Clostridium immunis*, a member of the *Lachnoclostridium*, is known to protect against colitis. This fact fits well with our data indicating that *Lachnoclostridium* was present at lower abundances after DSS treatment[34]. Interestingly, we also observed an increase in the *Prevotella sp.* in DSS-treated animals for both the colon content and mucus. *Prevotella* are considered as beneficial with regard to inflammatory

conditions in the gut[35-37]. Thus, DSS treatment might not only disturb the existing microbiota, but also induce a microbial community that counteracts the inflammatory reaction induced by tissue injury, which represents an interesting new aspect of the refined model of chronic DSS colitis.

In addition to changes between DSS-treated and control animals, we observed significant functional differences (KEGG metabolic pathways) between our sample types, i.e. cecum content, colon content, and colon mucus. This is different to previous studies that mostly relied on samples from feces or flushed cecum and colon content. This study segregated the different bacterial communities by separately sampling the cecum and colon content as well as colon mucus. Since the metabolic functions of bacteria in cecum and colon content were similar, this study confirmed the ability for recovery and resilience of these functions in the intestinal microbiota. These results are supported by Glymenaki *et al*. (2017), showing that despite changes in microbial composition, microbial functional pathways were stable before and during the development of mucosal inflammation[38]. These authors used the PICRUSt algorithm (Phylogenetic Investigation of Communities by Reconstruction of Unobserved States) to infer functional potential from identified OTUs[39]. PICRUSt is a method to predict the metabolic potential of the intestinal microbiota; however, it does not assess the truly present functions in the sample. Notably, in the present study, the microbial protein abundance was assessed using mass spectrometric analysis and therefore provided proof for the actual presence of the respective bacterial functional proteins.

Several metabolic pathways representing an altered abundance showed no statistical significance, which could be explained by the great dynamic range of microbial species abundance. Furthermore, the application of relative label-free protein quantification resulted in high variabilities of the identified protein groups, resulting in lower quantification sensitivity.

In order to quantify the association of the relative bacterial abundance (assessed by 16S rRNA amplicon sequencing) with metabolic functions of the intestinal microbiota (assessed by metaproteomics), we performed a correlation analysis. During inflammation, the mucus layer is degraded, providing an essential source of carbohydrates[40]. Therefore, we hypothesized that the carbohydrate metabolism was changed in the microbiota of DSS-treated animals. In fact, we observed a significant reduction in the general metabolic pathway of carbon metabolism as well as a significant decrease of Firmicutes, which are generally considered to metabolize carbohydrates, in the colon mucus. In contrast, the abundance of Proteobacteria (i.e. *Desulfovibrio*) was positively associated with the carbon metabolism. In general, *Desulfovibrio* is a prominent sulfate-reducing gut bacterium that is known to shape the response of a microbiota[41].

Biotin is as an essential cofactor involved in many metabolic processes, including membrane lipid synthesis, replenishment of the tricarboxylic acid cycle, and amino acid metabolism[42]. *Lachnoclostridium* showed a negative correlation with biotin in the cecum content while indicating a positive correlation with both vitamin B6 metabolism and tryptophan metabolism in the colon mucus. This finding may also suggest that more vitamin B6, a cofactor for aminotransferases, is needed for an increase in tryptophan metabolism[43].

In accordance with previous findings, a significant increase of the clinical score was observed in DSS-treated mice that were mainly due to diarrhea and colonic hemorrhage[19]. In addition, the Pearson correlation analysis indicated that the metaproteome data might be used to predict severe morphological changes (indexed by clinical and histological scores) during DSS administration. Our findings further support the hypothesis that functional changes in the distal colon caused by DSS treatment were far more pronounced in the mucus-associated microbiota than in the microbiota present in the distal colon content. This underlines the importance to sample not only feces or flushed cecum and colon content, but also colon mucus. To further characterize the refined model of DSS colitis used in this study, future studies will concentrate on the ability of the intestinal microbiota for recovery and resilience after chronic inflammation.

In conclusion, we found clear evidence that DSS treatment and the ensuing inflammatory response is accompanied by alterations in the composition as well as the function of the bacterial community at different taxonomic levels. How these changes relate to tissue inflammation and potentially perpetuate a dysregulated and chronic inflammatory response has to be clarified in future studies.

SUPPORTING INFORMATION

The following supporting information is available free of charge at ACS website

http://pubs.acs.org

- Supporting information: Supporting tables and figures

-Supporting Information Table S3: Omics data. 16S rRNA gene sequencing read counts and normalized abundances of identified protein groups from metaproteomic analysis.

- Supporting Information Table S4: Multi-level pattern analysis data for indicator species

ACKNOWLEDGEMENTS

We are acknowledging Kathleen Eismann (UFZ Department of Molecular Systems Biology) for her skilled technical assistance in protein sample preparation. The German Research

Foundation (DFG) with the Priority Program (SPP 1656) entitled “Intestinal Microbiota – a Microbial Ecosystem at the Edge between Immune Homeostasis and Inflammation” is acknowledged for funding.

CONFLICT OF INTEREST

There are no conflicts of interest to declare.

AUTHOR CONTRIBUTIONS

U.S., S.H., M.vB., N.J. and J.L. designed the study. U.S., M.H., K.W., S.H. performed the mouse experiments. S.H., N.J. and M.vB. performed the metaproteome analysis. S.H., M.H., U.S. and N.J. analyzed the data. All authors substantially contributed in the discussion of the data and are involved in writing the manuscript.

REFERENCES

1. Flint, H.J., Scott, K.P., Louis, P. & Duncan, S.H. The role of the gut microbiota in nutrition and health. *Nat Rev Gastroenterol Hepatol* **9**, 577-589 (2012).
2. Chubukov, V., Gerosa, L., Kochanowski, K. & Sauer, U. Coordination of microbial metabolism. *Nat Rev Microbiol* **12**, 327-340 (2014).
3. Odamaki, T. et al. Age-related changes in gut microbiota composition from newborn to centenarian: a cross-sectional study. *BMC microbiology* **16**, 90 (2016).
4. Sands, B.E. Inflammatory bowel disease: past, present, and future. *J Gastroenterol* **42**, 16-25 (2007).
5. Podolsky, D.K. Inflammatory bowel disease. *N Engl J Med* **347**, 417-429 (2002).
6. Kaser, A., Zeissig, S. & Blumberg, R.S. Inflammatory bowel disease. *Annu Rev Immunol* **28**, 573-621 (2010).
7. Li, J., Butcher, J., Mack, D. & Stintzi, A. Functional impacts of the intestinal microbiome in the pathogenesis of inflammatory bowel disease. *Inflamm Bowel Dis* **21**, 139-153 (2015).
8. Becker, C., Neurath, M.F. & Wirtz, S. The Intestinal Microbiota in Inflammatory Bowel Disease. *ILAR journal / National Research Council, Institute of Laboratory Animal Resources* **56**, 192-204 (2015).
9. Erickson, A.R. et al. Integrated metagenomics/metaproteomics reveals human host-microbiota signatures of Crohn's disease. *Plos One* **7**, e49138 (2012).
10. Bang, B. & Lichtenberger, L.M. Methods of inducing inflammatory bowel disease in mice. *Current protocols in pharmacology*, 5.58. 51-55.58. 42 (2016).
11. Chassaing, B., Aitken, J.D., Malleshappa, M. & Vijay-Kumar, M. Dextran sulfate sodium (DSS)-induced colitis in mice. *Current protocols in immunology*, 15.25. 11-15.25. 14 (2014).
12. Gkouskou, K.K., Deligianni, C., Tsatsanis, C. & Eliopoulos, A.G. The gut microbiota in mouse models of inflammatory bowel disease. *Frontiers in cellular and infection microbiology* **4**, 28 (2014).
13. Schaubeck, M. et al. Dysbiotic gut microbiota causes transmissible Crohn's disease-like ileitis independent of failure in antimicrobial defence. *Gut* **65**, 225-237 (2016).
14. Petriz, B.A. & Franco, O.L. Metaproteomics as a Complementary Approach to Gut Microbiota in Health and Disease. *Frontiers in chemistry* **5**, 4 (2017).

15. Franzosa, E.A. et al. Sequencing and beyond: integrating molecular 'omics' for microbial community profiling. *Nat Rev Microbiol* **13**, 360-372 (2015).
16. Oberbach, A. et al. Metabolic in Vivo Labeling Highlights Differences of Metabolically Active Microbes from the Mucosal Gastrointestinal Microbiome between High-Fat and Normal Chow Diet. *J Proteome Res* **16**, 1593-1604 (2017).
17. Wissenbach, D.K. et al. Optimization of metabolomics of defined in vitro gut microbial ecosystems. *International journal of medical microbiology : IJMM* **306**, 280-289 (2016).
18. Haange, S.B. & Jehmlich, N. Proteomic interrogation of the gut microbiota: potential clinical impact. *Expert review of proteomics* **13**, 535-537 (2016).
19. Hoffmann, M. et al. A refined and translationally relevant model of chronic DSS colitis in BALB/c mice. *Lab Anim* **0**, 0023677217742681.
20. Haange, S.B. et al. Metaproteome analysis and molecular genetics of rat intestinal microbiota reveals section and localization resolved species distribution and enzymatic functionalities. *J Proteome Res* **11**, 5406-5417 (2012).
21. Caporaso, J.G. et al. QIIME allows analysis of high-throughput community sequencing data. *Nature methods* **7**, 335-336 (2010).
22. DeSantis, T.Z. et al. Greengenes, a chimera-checked 16S rRNA gene database and workbench compatible with ARB. *Appl Environ Microbiol* **72**, 5069-5072 (2006).
23. Hochberg, Y. & Benjamini, Y. More powerful procedures for multiple significance testing. *Statistics in medicine* **9**, 811-818 (1990).
24. Ihaka, R. & Gentleman, R. R: A Language for Data Analysis and Graphics. *Journal of Computational and Graphical Statistics* **5**, 299-314 (1996).
25. Kanehisa, M. & Goto, S. KEGG: kyoto encyclopedia of genes and genomes. *Nucleic Acids Res* **28**, 27-30 (2000).
26. Dufrene, M. & Legendre, P. Species assemblages and indicator species: The need for a flexible asymmetrical approach. *Ecol Monogr* **67**, 345-366 (1997).
27. La Scola, B., Mallet, M.N., Grimont, P.A. & Raoult, D. Description of Afipia birgiae sp. nov. and Afipia massiliensis sp. nov. and recognition of Afipia felis genospecies A. *Int J Syst Evol Microbiol* **52**, 1773-1782 (2002).
28. Hoffmann, M. et al. Therapeutic efficacy of a combined sage and bitter apple phytopharmaceutical in chronic DSS-induced colitis. *Scientific reports* **7**, 14214 (2017).
29. Schwab, C. et al. Longitudinal study of murine microbiota activity and interactions with the host during acute inflammation and recovery. *Isme J* **8**, 1101-1114 (2014).
30. Berry, D. et al. Intestinal Microbiota Signatures Associated with Inflammation History in Mice Experiencing Recurring Colitis. *Front Microbiol* **6**, 1408 (2015).
31. Li, M., Wu, Y., Hu, Y., Zhao, L. & Zhang, C. Initial gut microbiota structure affects sensitivity to DSS-induced colitis in a mouse model. *Science China. Life sciences* **61**, 762-769 (2018).
32. Munyaka, P.M., Rabbi, M.F., Khafipour, E. & Ghia, J.E. Acute dextran sulfate sodium (DSS)-induced colitis promotes gut microbial dysbiosis in mice. *Journal of basic microbiology* **56**, 986-998 (2016).
33. Li, M., Wu, Y., Hu, Y., Zhao, L. & Zhang, C. Initial gut microbiota structure affects sensitivity to DSS-induced colitis in a mouse model. *Science China. Life sciences* (2017).
34. Surana, N.K. & Kasper, D.L. Moving beyond microbiome-wide associations to causal microbe identification. *Nature* **552**, 244-247 (2017).
35. Dillon, S.M. et al. Gut dendritic cell activation links an altered colonic microbiome to mucosal and systemic T-cell activation in untreated HIV-1 infection. *Mucosal immunology* **9**, 24-37 (2016).
36. Ley, R.E. Gut microbiota in 2015: Prevotella in the gut: choose carefully. *Nat Rev Gastroenterol Hepatol* **13**, 69-70 (2016).
37. Scher, J.U. et al. Expansion of intestinal Prevotella copri correlates with enhanced susceptibility to arthritis. *eLife* **2**, e01202 (2013).

38. Glymenaki, M. et al. Stability in metabolic phenotypes and inferred metagenome profiles before the onset of colitis-induced inflammation. *Scientific reports* **7**, 8836 (2017).
39. Langille, M.G. et al. Predictive functional profiling of microbial communities using 16S rRNA marker gene sequences. *Nat Biotechnol* **31**, 814-821 (2013).
40. Johansson, M.E. et al. Composition and functional role of the mucus layers in the intestine. *Cellular and molecular life sciences : CMLS* **68**, 3635-3641 (2011).
41. Rey, F.E. et al. Metabolic niche of a prominent sulfate-reducing human gut bacterium. *Proc Natl Acad Sci U S A* **110**, 13582-13587 (2013).
42. Salaemae, W., Booker, G.W. & Polyak, S.W. The Role of Biotin in Bacterial Physiology and Virulence: a Novel Antibiotic Target for Mycobacterium tuberculosis. *Microbiology spectrum* **4** (2016).
43. Rosenberg, J., Ischebeck, T. & Commichau, F.M. Vitamin B6 metabolism in microbes and approaches for fermentative production. *Biotechnol Adv* **35**, 31-40 (2017).

TABLE OF CONTENTS GRAPHIC (TOC)

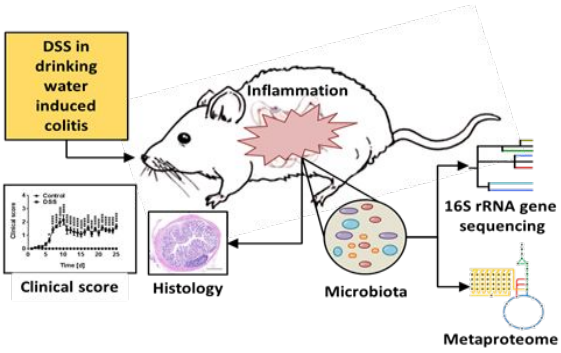

FIGURE LEGENDS

Figure 1: Chronic colitis was induced in BALB/c mice by administration of 2 % DSS in drinking water for 7 days followed by 10 days of 1 % DSS and another 7 days of 2 % DSS. Animals receiving normal drinking water represented the healthy control. Clinical score (**A**), body weight (**B**) stool consistency (**C**) and colonic hemorrhage (**D**) were evaluated daily and are shown as mean ± SEM for 12 animals per group. Post mortem, the colon was dissected and the colon length was determined for 12 animals per group (**E**). The median of individual data points is indicated. * $P<0.05$, ** $P<0.01$, *** $P<0.001$, **** $P<0.0001$ vs. the healthy control group, n=12

Figure 2: Chronic colitis was induced in BALB/c mice by administration of 2 % DSS in drinking water for 7 days followed by 10 days of 1 % DSS and another 7 days of 2 % DSS. Animals receiving normal drinking water represented the healthy control. (**A**) Exemplary images of hematoxylin and eosin (H&E), anti-MPO, anti-F4/80, or anti-CD3 stained tissue sections (3 µm) of the distal colon; scale bar (H&E): 500 µm; scale bar (immunofluorescence): 100 µm. (**B**) The histopathological score was determined based on H&E-stained sections of the distal colon from 12 animals per group. Cross sections of the distal colon (two sections/mouse) stained for MPO (**C**), the macrophage marker F4/80 (**D**), and the T cell marker CD3 (**E**) were digitized with a slide scanner (Zeiss AxioScan.Z1). Expression was quantified using the ImageJ software program and is shown as marker-positive area relative to the DAPI-positive area. The median of individual data points is indicated. * $P<0.05$, ** $P<0.01$, *** $P<0.001$ vs. the control group, n=12

Figure 3: 16S rRNA gene analysis. PCA of abundance of operational taxonomic units (OTUs) (**A**). NMDS plots for each sampled locality of OTUs abundance. P values were calculated using the input data for NMDS calculation and performing a *Permanova* analysis using the *adonis* function from the vegan R package (**B**). Mean relative abundances of phyla based on 16S rRNA gene reads (**C**), n=8 except for DSS-treated distal colon mucus (n=7)

Figure 4: The heat-map depicts significant changes in abundance of taxa from 16S rRNA gene sequencing analysis. *P* values have been adjusted for multi-testing using the Benjamini-Hochberg method, n=8 except for DSS-treated distal colon mucus (n=7)

Figure 5: Metaproteomics data of the gut microbiota. Principal component analysis of COG function (**A**). NMDS plots of metaproteomics data. *P* values were calculated using the input data for NMDS calculation with *adonis* function from the vegan R package (**B**). Protein group enrichment analysis of functional pathways. Log_2 fold change is: ** $P<0.01$, * $P<0.05$, ns =not significant. *P* values are adjusted according to Benjamini-Hochberg, n=12, except for DSS-treated distal colon content (n=10)

Figure 6: Correlation of relative abundance of bacterial phyla and genera from the 16S rRNA gene sequencing data (top) as well as the relative number of protein groups from metabolic functional pathways of the metaproteomic analysis (bottom) with the clinical and histological score. Only Pearson correlation scores of significance (P<0.01) are depicted.

Figure 7: Correlation of relative number of protein groups of functional pathways from the microbiota with the relative abundance of bacterial taxa as determined by 16S rRNA gene sequencing for the cecum content, distal colon content and distal colon mucus. Only Pearson correlation scores of significance (P<0.01) are depicted.

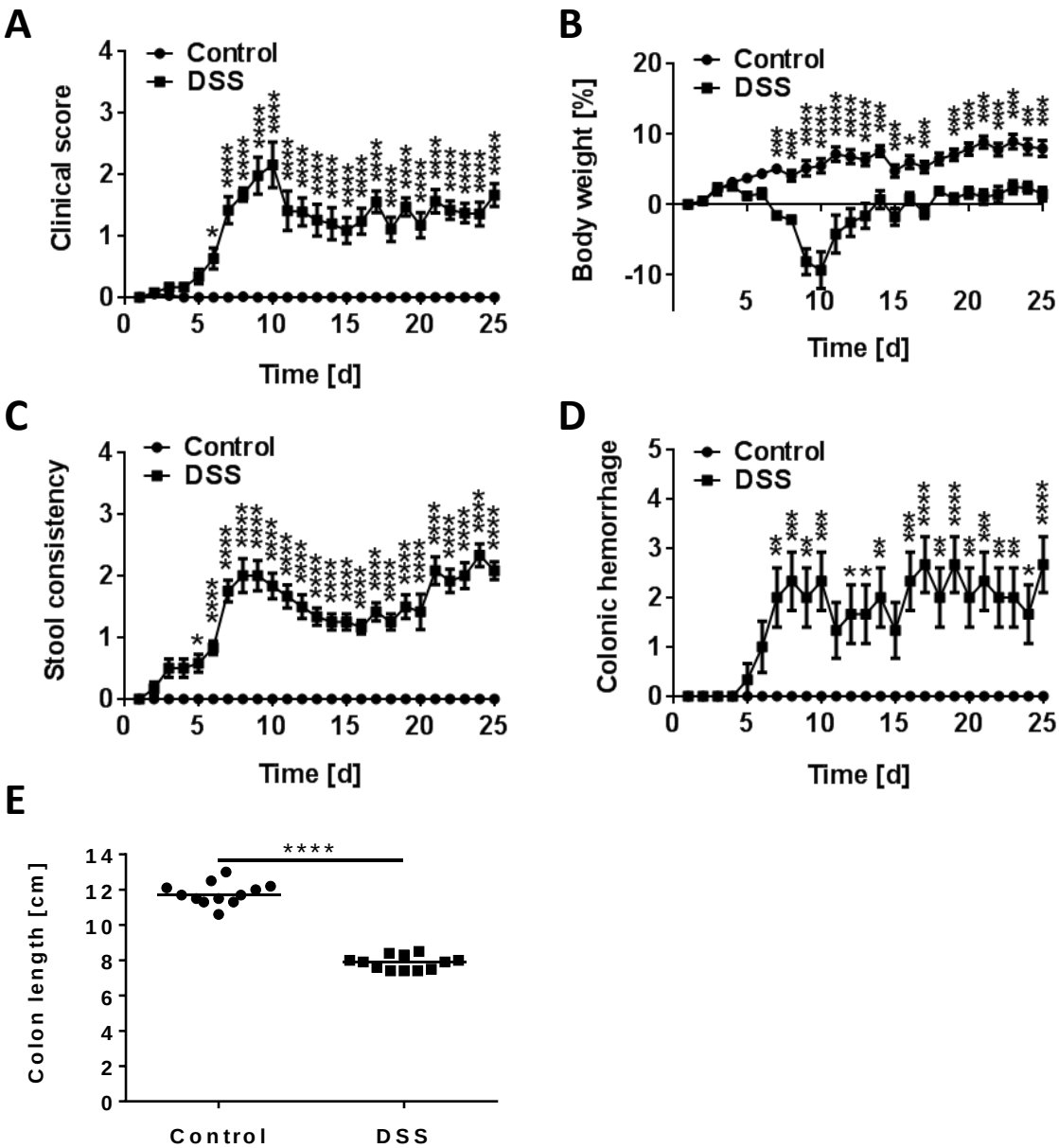
A
Control
DSS
Clinical score
Time [d]
B
Control
DSS
Body weight [%]
Time [d]
C
Control
DSS
Stool consistency
Time [d]
D
Control
DSS
Colonic hemorrhage
Time [d]
E
****
Colon length [cm]
Control
DSS

Figure 1

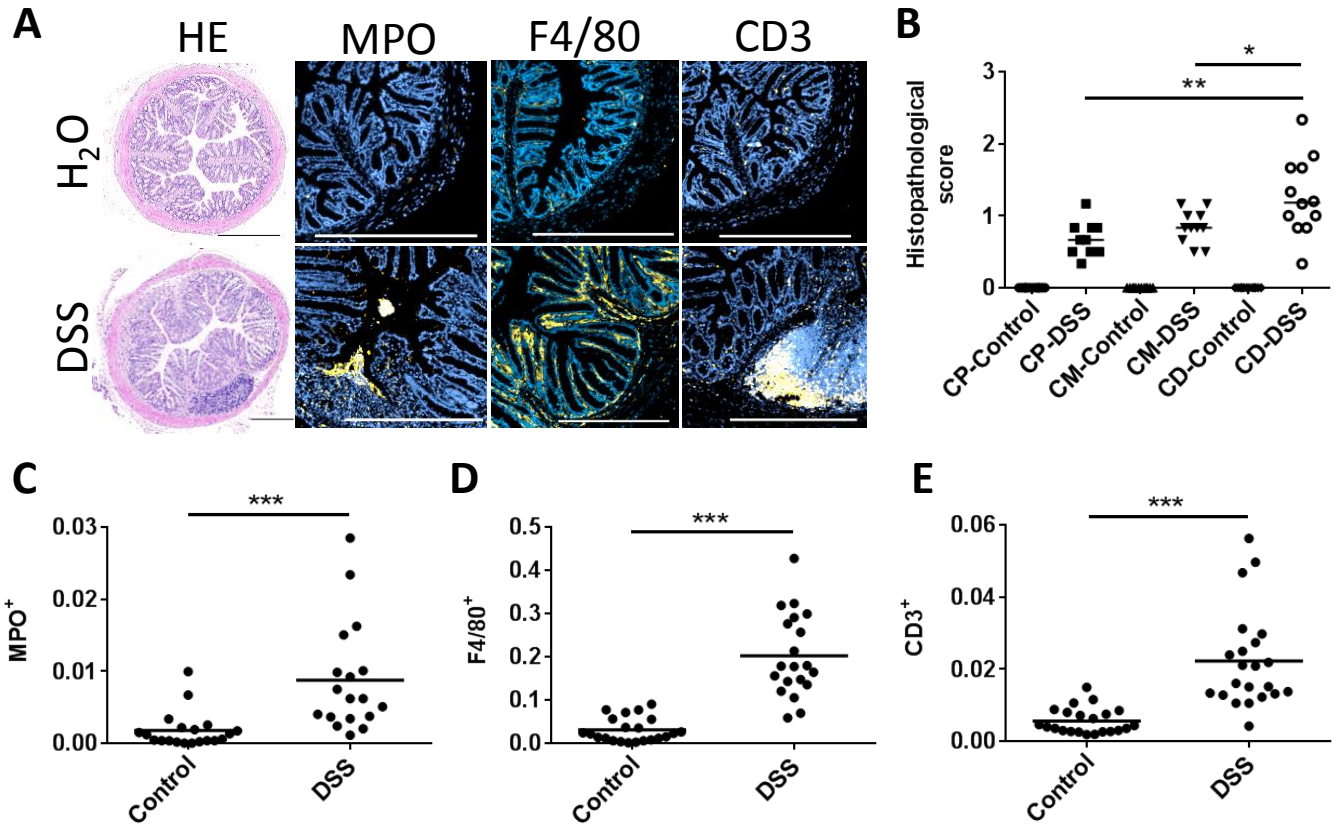
A
HE
MPO
F4/80
CD3
H_2O
DSS
B
Histopathological score
CP-Control
CP-DSS
CM-Control
CM-DSS
CD-Control
CD-DSS
C
MPO^+
Control
DSS
D
$F4/80^+$
E
$CD3^+$

Figure 2

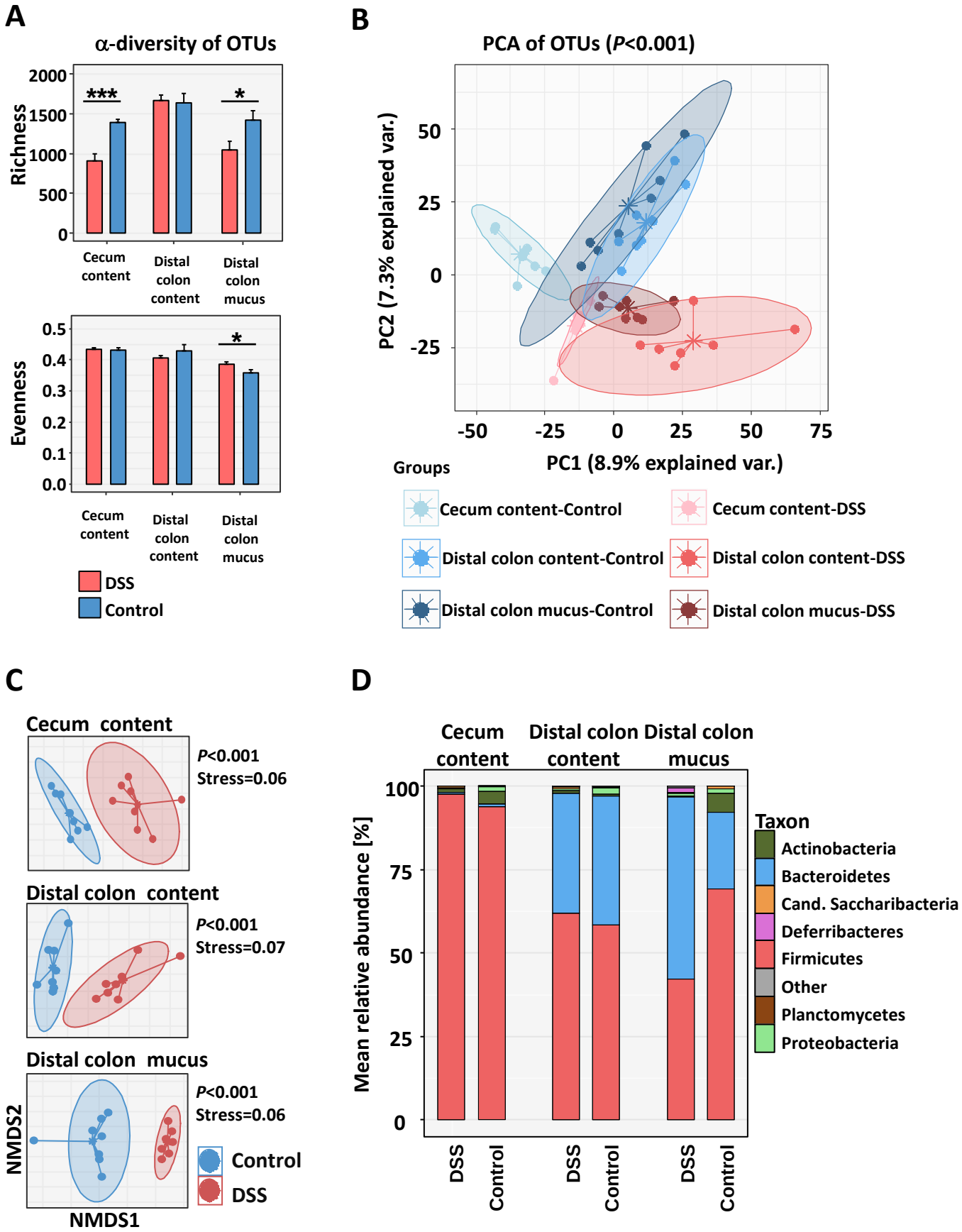
A
α-diversity of OTUs
Richness
2000
1500
1000
500
0
***
*
Cecum content
Distal colon content
Distal colon mucus
Evenness
0.5
0.4
0.3
0.2
0.1
0.0
*
Cecum content
Distal colon content
Distal colon mucus
DSS
Control
B
PCA of OTUs (P<0.001)
PC2 (7.3% explained var.)
50
25
0
-25
-50
-25
0
25
50
75
PC1 (8.9% explained var.)
Groups
Cecum content-Control
Cecum content-DSS
Distal colon content-Control
Distal colon content-DSS
Distal colon mucus-Control
Distal colon mucus-DSS
C
Cecum content
P<0.001
Stress=0.06
Distal colon content
P<0.001
Stress=0.07
Distal colon mucus
P<0.001
Stress=0.06
NMDS2
NMDS1
Control
DSS
D
Cecum content
Distal colon content
Distal colon mucus
Mean relative abundance [%]
100
75
50
25
0
DSS
Control
DSS
Control
DSS
Control
Taxon
Actinobacteria
Bacteroidetes
Cand. Saccharibacteria
Deferribacteres
Firmicutes
Other
Planctomycetes
Proteobacteria

Figure 3


Cecum content
Distal Colon content
Distal Colon mucus
Phylum
Actinobacteria
Bacteroidetes
Deferribacteres
Firmicutes
Proteobacteria
Spirochaetes
Class
Actinobacteria_class
Bacilli
Bacteroidia
Betaproteobacteria
Clostridia
Deltaproteobacteria
Sphingobacteriia
Spirochaetia
Order
Bacteroidales
Clostridiales
Coriobacteriales
Desulfovibrionales
Lactobacillales
Sphingobacteriales
Family
Catabacteriaceae
Clostridiaceae
Coriobacteriaceae
Lactobacillaceae
Oscillospiraceae
Planococcaceae
Porphyromonadaceae
Prevotellaceae
Rikenellaceae
Ruminococcaceae
Sphingobacteriaceae
Genus
Alistipes
Allobaculum
Bacteroides
Barnesiella
Catabacter
Clostridium
Denitrobacterium
Enterorhabdus
Erysipelatoclostridium
Lachnoclostridium
Lactobacillus
Marvinbryantia
Nubsella
Oscillibacter
Parabacteroides
Parvibacter
Pedobacter
Prevotella
Pseudoflavonifractor
Ruminococcus
DSS
Control
Log2 fc
p-value
[%]
Mean relative abundance
100%
1%
0
Log2 fold change (DSS/control)
9
0.2
-0.2
-9
Significance
P (BH adjusted)
1
<0.05
<0.01
<0.001

Figure 4

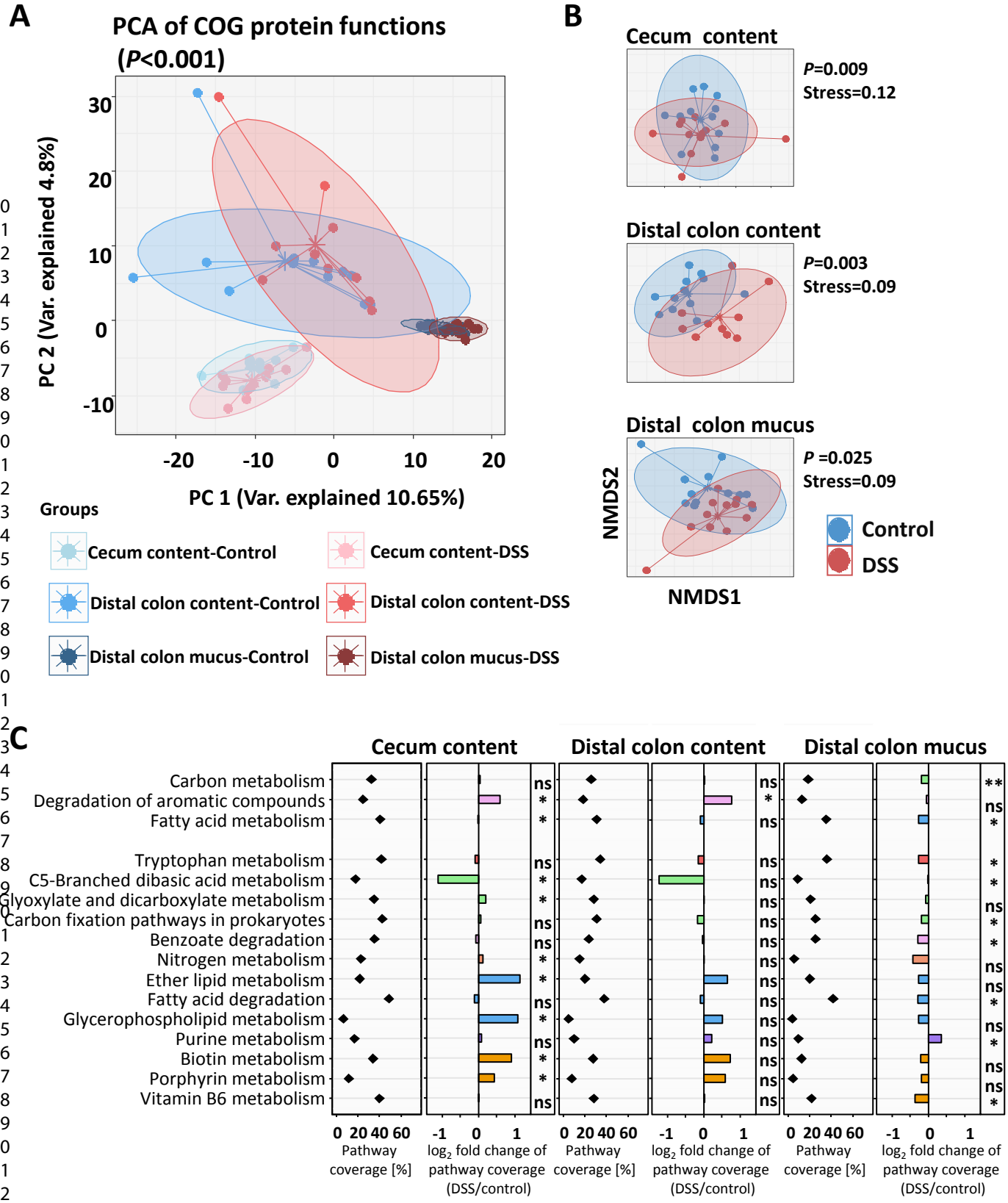
A
PCA of COG protein functions
(P<0.001)
PC 2 (Var. explained 4.8%)
PC 1 (Var. explained 10.65%)
30
20
10
0
-10
-20
-10
0
10
20
Groups
Cecum content-Control
Cecum content-DSS
Distal colon content-Control
Distal colon content-DSS
Distal colon mucus-Control
Distal colon mucus-DSS
B
Cecum content
P=0.009
Stress=0.12
Distal colon content
P=0.003
Stress=0.09
Distal colon mucus
P =0.025
Stress=0.09
NMDS2
NMDS1
Control
DSS
C
Cecum content
Distal colon content
Distal colon mucus
Carbon metabolism
Degradation of aromatic compounds
Fatty acid metabolism
Tryptophan metabolism
C5-Branched dibasic acid metabolism
Glyoxylate and dicarboxylate metabolism
Carbon fixation pathways in prokaryotes
Benzoate degradation
Nitrogen metabolism
Ether lipid metabolism
Fatty acid degradation
Glycerophospholipid metabolism
Purine metabolism
Biotin metabolism
Porphyrin metabolism
Vitamin B6 metabolism
ns
*
**
0 20 40 60
Pathway coverage [%]
-1 0 1
log2 fold change of pathway coverage (DSS/control)

Figure 5


Cecum content
Colon content
Colon mucus
Phylum
Actinobacteria
Deferribacteres
Firmicutes
Genus
Arthrobacter
Denitrobacterium
Enterorhabdus
Paraeggerthella
Parvibacter
Alistipes
Barnesiella
Nubsella
Parabacteroides
Pedobacter
Prevotella
Mucispirillum
Allobaculum
Catabacter
Clostridium
Dorea
Erysipelatoclostridium
Hydrogenoanaerobacterium
Johnsonella
Lachnoclostridium
Lactobacillus
Marvinbryantia
Planococcus
Pseudobutyrivibrio
Pseudoflavonifractor
Ruminiclostridium
Ruminococcus
Delftia
Stenotrophomonas
C H C H C H
Significant Pearson correlation scores (P< 0.01)
1
0.5
0
-0.5
-1
Non-significant
Phylum
Firmicutes
Actinobacteria
Bacteroidetes
Deferribacteres
Proteobacteria
Metabolism
Carbon.metabolism
Carbohydrate.metabolism
Lipid.metabolism
Amino.acid.metabolism
Metabolism.of.cofactors.and.vitamins
Metabolism.of.other.amino.acids
Metabolism.of.terpenoids.and.polyketides
Xenobiotics.biodegradation.and.metabolism
Biosynthesis.of.other.secondary.metabolites
Energy.metabolism
C = Clinical score
H = Histopathological score
Score
Cecum content
Colon content
Colon mucus
Pathway
Biosynthesis.of.amino.acids
Cysteine.and.methionine.metabolism
Tryptophan.metabolism
Betalain.biosynthesis
Flavone.and.flavonol.biosynthesis
Indole.alkaloid.biosynthesis
Glycolysis./.Gluconeogenesis
Carbon.metabolism
Carbon.fixation.pathways.in.prokaryotes
Lipopolysaccharide.biosynthesis
Other.glycan.degradation
alpha.Linolenic.acid.metabolism
Arachidonic.acid.metabolism
Ether.lipid.metabolism
Fatty.acid.degradation
Fatty.acid.metabolism
Primary.bile.acid.biosynthesis
Steroid.biosynthesis
Biotin.metabolism
Vitamin.B6.metabolism
beta.Alanine.metabolism
Biosynthesis.of.siderophore.group.nonribosomal.peptides
Geraniol.degradation
Polyketide.sugar.unit.biosynthesis
Terpenoid.backbone.biosynthesis
Tetracycline.biosynthesis
Benzoate.degradation
Chlorocyclohexane.and.chlorobenzene.degradation
Degradation.of.aromatic.compounds
Drug.metabolism...cytochrome.P450
Drug.metabolism...other.enzymes
Ethylbenzene.degradation
Fluorobenzoate.degradation
Metabolism.of.xenobiotics.by.cytochrome.P450
Styrene.degradation
Xylene.degradation
C H C H C H
ACS Paragon Plus Environment

Figure 6

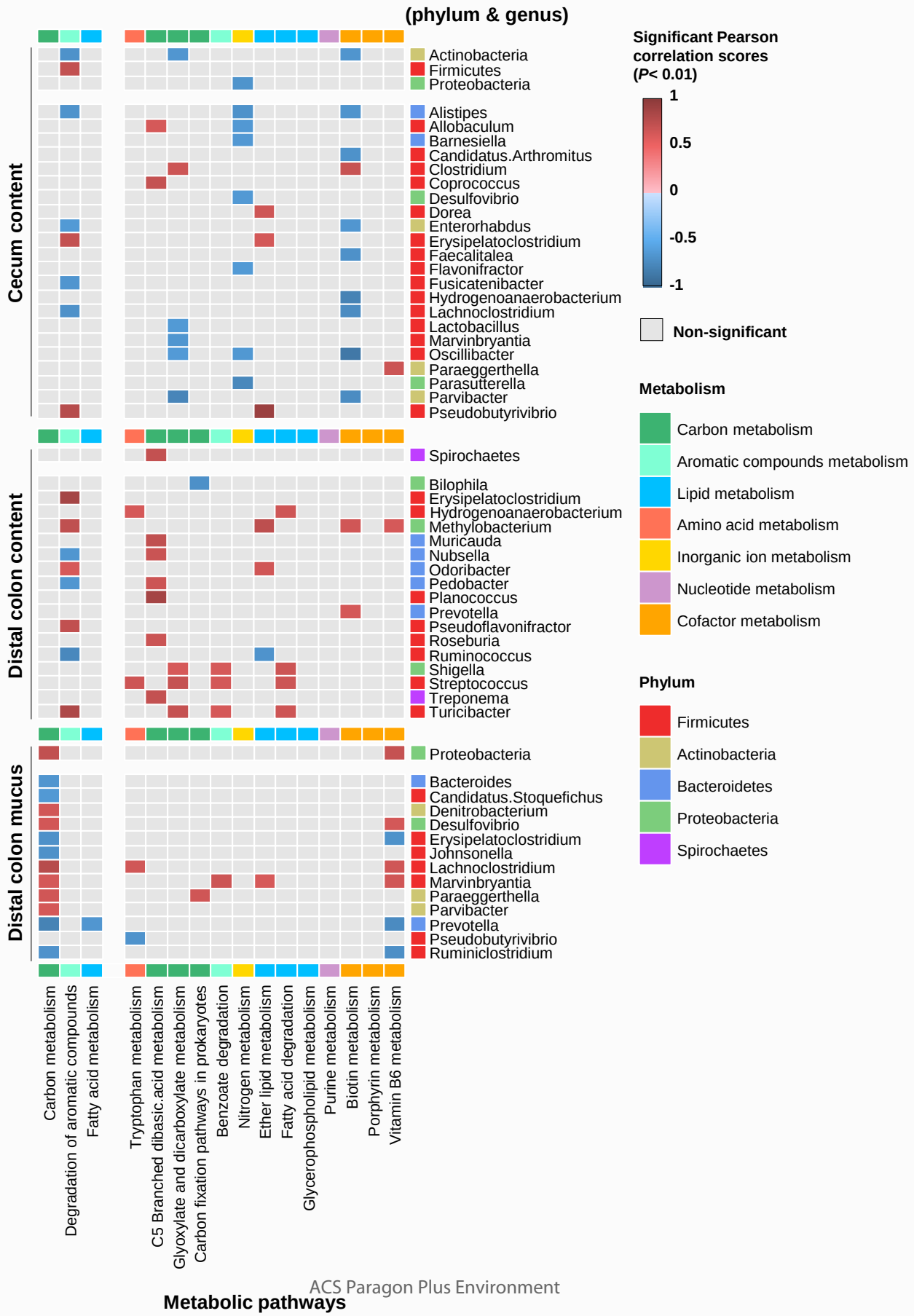
Taxa
(phylum & genus)
Cecum content
Distal colon content
Distal colon mucus
Actinobacteria
Firmicutes
Proteobacteria
Alistipes
Allobaculum
Barnesiella
Candidatus.Arthromitus
Clostridium
Coprococcus
Desulfovibrio
Dorea
Enterorhabdus
Erysipelatoclostridium
Faecalitalea
Flavonifractor
Fusicatenibacter
Hydrogenoanaerobacterium
Lachnoclostridium
Lactobacillus
Marvinbryantia
Oscillibacter
Paraeggerthella
Parasutterella
Parvibacter
Pseudobutyrivibrio
Spirochaetes
Bilophila
Erysipelatoclostridium
Hydrogenoanaerobacterium
Methylobacterium
Muricauda
Nubsella
Odoribacter
Pedobacter
Planococcus
Prevotella
Pseudoflavonifractor
Roseburia
Ruminococcus
Shigella
Streptococcus
Treponema
Turicibacter
Proteobacteria
Bacteroides
Candidatus.Stoquefichus
Denitrobacterium
Desulfovibrio
Erysipelatoclostridium
Johnsonella
Lachnoclostridium
Marvinbryantia
Paraeggerthella
Parvibacter
Prevotella
Pseudobutyrivibrio
Ruminiclostridium
Carbon metabolism
Degradation of aromatic compounds
Fatty acid metabolism
Tryptophan metabolism
C5 Branched dibasic.acid metabolism
Glyoxylate and dicarboxylate metabolism
Carbon fixation pathways in prokaryotes
Benzoate degradation
Nitrogen metabolism
Ether lipid metabolism
Fatty acid degradation
Glycerophospholipid metabolism
Purine metabolism
Biotin metabolism
Porphyrin metabolism
Vitamin B6 metabolism
Metabolic pathways
Significant Pearson correlation scores
(P< 0.01)
1
0.5
0
-0.5
-1
Non-significant
Metabolism
Carbon metabolism
Aromatic compounds metabolism
Lipid metabolism
Amino acid metabolism
Inorganic ion metabolism
Nucleotide metabolism
Cofactor metabolism
Phylum
Firmicutes
Actinobacteria
Bacteroidetes
Proteobacteria
Spirochaetes

Figure 7